Segmentation of Breast MRI Scans in the Presence of Bias Fields

Hossein Soleimani(✉), Jose Rincon, and Oleg V. Michailovich

University of Waterloo, Waterloo, Canada
{h3soleim,jrincon,olegm}@uwaterloo.ca

Abstract. Magnetic Resonance Imaging (MRI) is currently considered to be the most sensitive tool for imaging-based diagnostic and presurgical assessment of breast cancer. In addition to their valuable diagnostic contrasts, MRI scans also provide a superb delineation of breast anatomy, which facilitates a number of related clinical applications, among which are breast density estimation and bio-mechanical modeling of breast tissue. Such applications, however, require one to know the disposition of various types of the tissue, thus warranting the procedure of image segmentation. In the case of breast MRI, the latter is known to be a challenging problem due to the relatively complicate nature of measurement noises, which is particularly problematic to deal with in the presence of bias fields. Accordingly, in this work, we introduce a simple method that can be used to "gaussianize" the noise statistic, which allows the problem of image segmentation to be formulated in the form of a simple optimization problem. In this formulation, segmentation of breast MRI scans can be completed in only a few iterations as demonstrated by our experiments involving both *in silico* and *in vivo* MRI data.

Keywords: Breast MRI · Image segmentation · Bias fields · Numerical optimization

1 Introduction

Breast cancer is the most common malignancy diagnosed in women worldwide. Although the introduction of screening mammography has resulted in a massive reduction in the mortality rates of breast cancer, the efficacy of mammography remains limited due to its relatively low sensitivity. For this reason, for women at increased risk breast cancer, it is often necessary to use alternative screening technologies, among which is Magnetic Resonance Imaging (MRI). Particularly, MRI is currently recommended for screening asymptomatic women at high risk for breast cancer related to inherited genetic mutations, family history of breast carcinoma and some other risk factors [1]. Moreover, in addition to screening, breast MRI is routinely used in other clinical scenarios, such as preoperative assessment in women with newly diagnosed breast carcinoma [2].

The relatively high sensitivity of MRI to pathological changes in the breast is favorably complemented by its ability to accurately depict the breast anatomy.

F. Karray et al. (Eds.): ICIAR 2019, LNCS 11662, pp. 376–387, 2019.
https://doi.org/10.1007/978-3-030-27202-9_34

For this reason, breast MRI scans have been successfully used to facilitate a number of related clinical applications, including breast density estimation, prone-to-supine breast MRI registration and mammography-MRI image fusion. Whilst different in terms of their aims and outcomes, these applications share a common need for classification of image values according to various types of breast tissue the latter are supposed to depict. This classification is usually formulated as a problem of *image segmentation* [3,4], which is in the focus of this work.

The problem of segmentation of breast MRI scans have been addressed in several studies using a range of different approaches, such as thresholding-based and gradient-based image segmentation, active contours, machine learning and others [5]. Thus, for example, an adaptation of the fuzzy c-means method with a specially designed kernel was proposed in [6], while a solution to the problem of segmentation of dermal and fibroglandular tissue by means of k-means clustering was described in [7]. An alternative use of the fuzzy c-means method, resulting in an adaptive and semi-automatic algorithm for segmentation of fibroglandular and adipose tissue, was introduced in [9]. In [8], a similar idea of semi-automatic segmentation was realized based on the method of region growing. Unfortunately, the manual selection of seed points as well as the relatively high computational complexity of this method somewhat weaken its otherwise excellent performance.

The recent advent and proliferation of the theory and tools of deep learning has substantially expanded the possibilities of image segmentation as well. Thus, for example, a particular architecture of deep neural networks (DNN), known as U-net, was used to segment fibroglandular and adipose tissues in [10]. It has been shown that the use of DNN allowed a substantial increase in the accuracy of image segmentation, notably outperforming many alternative approaches. It should be noted, however, that the performance of DNNs usually improves *pro rata* with the size of training sets (e.g., manually segmented MRI scans, in the case at hand). Thus, generalizing the method of [10] to a wide range of different densities and geometries of the breast could be potentially problematic.

When searching for relatively simple yet robust methods of segmentation of breast MRI scans, statistical methods based on use of *mixture models* deserve special noting. In particular, the assumption on image values to obey a Gaussian Mixture Model (GMM) was exploited in [11,12]. In this case, the GMM model is typically fitted by means of the Expectation Maximization (EM) algorithm [13], properly modified to account for spatial dependencies between same-class labels (using, e.g., the Markov Random Field model [12]).

For relatively high values of signal-to-noise ratio (SNR), the GMM is known to provide an adequate approximation of the probability distribution of breast MRI scans. At low SNR, however, the quality of this statistical model is known to plummet, causing notable segmentation artifacts. To resolve this problem, in the present work, we consider the use of *Rician* Mixture Modeling (RMM) [14], which is known to be a more natural and accurate statistical description in the case of MRI. To avoid dealing with the generally complex nature of RMM fitting, we introduce a simple "gaussianization" procedure which effectively reduces the Rician case to a Gaussian one. Moreover, the proposed method can explicitly

account for the effect of bias fields [17], ultimately leading to a straightforward optimization problem. The latter is shown to admit a computationally efficient solution, which can be found in just a few iterations. What is more important is that the proposed algorithm has been observed to outperform GMM-based segmentation at low SNR (as expected). This result is confirmed using experiments with both phantom (*in silico*) and real-life (*in vivo*) data.

The remainder of the paper is organized as follows. The proposed method and its numerical implementation are summarized in Sect. 2, while Sect. 3 presents the results of our numerical experiments. Finally, Sect. 4 concludes the paper with a discussion of its principal findings.

2 Proposed Method

2.1 Image Preprocessing

To set the notations, let $\Omega \in \mathbb{R}^3$ be a volumetric image domain over with an MRI scan $F : \Omega \to \mathbb{R}$ is assumed to be defined. The scan F is also assumed to be contaminated by a bias field $B : \Omega \to \mathbb{R}$, the effect of which is usually considered to be multiplicative. Consequently, in the absence of other artifacts and noises, the corresponding observed image G could be modeled as

$$G(\mathbf{r}) = F(\mathbf{r})B(\mathbf{r}), \quad \mathbf{r} \in \Omega. \tag{1}$$

In practical settings, G is always contaminated by Rician noise, which leads to a relatively complex analysis in the presence of B. To simplify the model, one can redefine (1) in the logarithmic domain as

$$g(\mathbf{r}) = \mathcal{R}_{\mathcal{L}}\left\{f(\mathbf{r}) + b(\mathbf{r})\right\}, \quad \mathbf{r} \in \Omega, \tag{2}$$

with g, f and b standing for $\log G$, $\log F$ and $\log B$, respectively, and with $\mathcal{R}_{\mathcal{L}}\{\cdot\}$ being a symbolic representation of the effect of the log-transformed Rician noise. The latter can be shown to behave similarly to a Gaussian noise, except for the presence of occasional "spikes", which can be attributed to the relatively large mass of the left-side tail of a log-Rician distribution. In its Subplot A, Fig. 1 depicts some examples of Rician probability densities $\mathcal{R}(x \,|\, \sigma, \nu)$ for $\sigma = 1$ and $\nu = 1, 2, 3$. Note how the shapes of the densities transform from asymmetric to Gaussian-like as ν increases. Subplot B of the same figure, on the other hand, shows the corresponding log-Rician probability densities $\mathcal{R}_{\mathcal{L}}(y \,|\, \sigma, \nu)$ (with $y = \log x$). Note that, for all ν, the densities have a Gaussian-like appearance, with the exception of their heavy left tail.

Clearly, dealing with the log-Rician noise offers few advantages over the Rician case, unless the former is properly "gaussianized" so that $\mathcal{R}_{\mathcal{L}}\left\{f(\mathbf{r}) + b(\mathbf{r})\right\}$ can be approximately replaced with $f(\mathbf{r}) + b(\mathbf{r}) + u(\mathbf{r})$, where $u(\mathbf{r})$ obeys a Gaussian distribution. Note that such "gaussianization" should, in fact, be able to suppress the impulsive component of the log-Rician noise. Such a result can be achieved by means of the procedure of *outlier shrinkage* as given by

$$g(\mathbf{r}) \mapsto g(\mathbf{r}) - \mathcal{S}_{\lambda}\left\{g(\mathbf{r}) - \bar{g}(\mathbf{r})\right\}, \quad \forall \mathbf{r} \in \Omega, \tag{3}$$

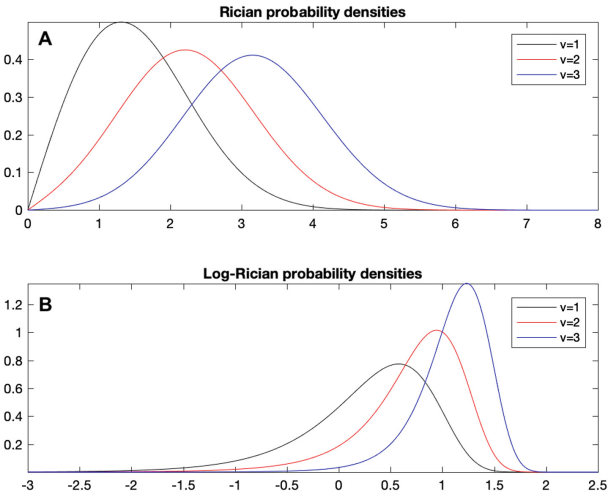

Fig. 1. (Subplot A) Rician probability densities $\mathcal{R}(x\,|\,\sigma,\nu)$ for $\sigma = 1$ and $\nu = 1, 2, 3$; (Subplot B) Corresponding log-Rician densities $\mathcal{R}_{\mathcal{L}}(y\,|\,\sigma,\nu)$, with $y = \log x$.

where $\bar{g}$ stands for a median-filtered version of g[1], while $\mathcal{S}_\lambda$ denotes the operator of soft thresholding given by

$$\mathcal{S}_\lambda(z) = \min(z + \lambda, 0) + \max(z - \lambda, 0),$$

where $\lambda > 0$ is a predefined threshold value.

The action of outlier shrinkage is straightforward. With the original image f being a piece-wise smooth function and b being a smooth field, the residuals $g - \bar{g}$ can be reasonably assumed to be dominated by noise. When subjected to soft thresholding, the noise retains its largest values which are likely to be associated with its impulsive ("spiky") component. Subsequently, the latter is subtracted from g, thus making the residual noise to behave in a nearly Gaussian manner.

Despite its conceptual and computational simplicity, the procedure of outlier shrinkage has demonstrated considerable efficacy for properly set values of λ. In this work, the latter has been set to be equal two times the median absolute deviation (MAD) of the residual $g - \bar{g}$ [15].

2.2 Two-Class Segmentation Model

The anatomy of breast is fairly complex. However, when it comes to the T1/T2 contrasts, which are typically used in breast MRI, there are two main tissue classes that are usually targeted by image segmentation algorithms. These classes correspond to fibroglandular and adipose tissue, which we will refer below to as

[1] In practical computations, a 3×3 median filter has proven to be an adequate choice.

the dense and fat tissues, respectively[2]. Accordingly, in what follows, the problem of image segmentation will be formulated for a two-class scenario. In this case, the objective of image segmentation becomes to partition the domain Ω into two mutually exclusive subdomains Ω_d and Ω_f (with $\Omega = \Omega_d \cup \Omega_f$ and $\Omega_d \cap \Omega_f = \emptyset$) associated with the dense and fat tissues, respectively. Such a partition can, in turn, be described in terms of an *partition function* $\xi : \Omega \to \{0, 1\}$ given by

$$\xi(\mathbf{r}) = \begin{cases} 1, & \mathbf{r} \in \Omega_d \\ 0, & \mathbf{r} \in \Omega_f. \end{cases}$$

Consequently, the problem of image segmentation can be equivalently formulated as a problem of estimation of function ξ.

One way to formulate the above estimation problem is by taking advantage of the effect of outlier shrinkage, which guarantees the residual noise contaminating g is approximately additive white Gaussian noise (AWG). In this case, it seems reasonable to assume the class-conditional probability densities $p(g(\mathbf{r}) \,|\, \mathbf{r} \in \Omega_d)$ and $p(g(\mathbf{r}) \,|\, \mathbf{r} \in \Omega_f)$ to be Gaussian with their means equal to $\mu_d + b(\mathbf{r})$ and $\mu_f + b(\mathbf{r})$, respectively. Under this assumption, the problem of estimation of ξ can be expressed as an optimization problem of the form

$$\min_{\xi, \mu_d, \mu_f, b} \left\{ \lambda_d \sum_{\mathbf{r} \in \Omega} \xi(\mathbf{r}) |g(\mathbf{r}) - \mu_d - b(\mathbf{r})|^2 + \lambda_f \sum_{\mathbf{r} \in \Omega} (1 - \xi(\mathbf{r})) |g(\mathbf{r}) - \mu_f - b(\mathbf{r})|^2 \right\}$$
$$\text{s.t. } \xi(\mathbf{r}) \in \{0, 1\}, \ \forall \mathbf{r} \in \Omega, \tag{4}$$

for some regularization parameters $\lambda_d, \lambda_f > 0$. It is important to emphasize that, in (4), both μ_d and μ_f as well as the bias field b are treated as optimization variables, similarly to ξ.

The problem defined by (4) is a non-convex integer optimization problem, a solution to which would have been quite difficult to find in general. To overcome this difficulty, one can try to "relax" the problem by letting the values of $\xi(\mathbf{r})$ be anywhere within the interval $[0, 1]$ (instead of being trapped at either 0 or 1), while restricting the optimal ξ^* to the class of piece-wise smooth functions. This can be accomplished by minimizing the value of the *total variation* (TV) semi-norm of ξ that is given by

$$\|\xi\|_{\text{TV}} = \sum_{\mathbf{r} \in \Omega} |\nabla \xi(\mathbf{r})|,$$

where $\nabla \xi$ denotes the (discrete) gradient of ξ and $|\nabla \xi(\mathbf{r})|$ stands for its magnitude at position $\mathbf{r}$. Consequently, the resulting minimization problem acquires the following form [18]

[2] In the absence of contrast enhancement, dermal and tumorous tissues have a visual appearance similar to that of dense tissue. For this reason, tumors are often included in the "dense" class.

$$\min_{\xi,\mu_d,\mu_f,b}\Bigg\{\lambda_d\sum_{\mathbf{r}\in\Omega}\xi(\mathbf{r})|g(\mathbf{r})-\mu_d-b(\mathbf{r})|^2+\lambda_f\sum_{\mathbf{r}\in\Omega}(1-\xi(\mathbf{r}))|g(\mathbf{r})-\mu_f-b(\mathbf{r})|^2+ \\ +\ \|\xi\|_{\mathrm{TV}}+I_{[0,1]}(\xi)\Bigg\}, \tag{5}$$

where $I_{[0,1]}$ stands for the indicator function of the closed interval $[0,1]$ that is given by

$$I_{[0,1]}(z)=\begin{cases}0, & 0\le z\le 1,\\ \infty, & \text{otherwise}\end{cases}.$$

Additionally, one can also take advantage of the fact that, in practice, the bias field b is a smooth slowly varying function, which can approximated by a polynomial of a relatively low order. Specifically, let $\{\varphi_k\}_{k=0}^{K}$ be a set of polynomials of orders $0,1,\ldots,K$. Then, with $\Phi_{i,j,k}(\mathbf{r})=\Phi_{i,j,k}(\mathbf{r}_1,\mathbf{r}_2,\mathbf{r}_3)=\varphi_i(\mathbf{r}_1)\varphi_j(\mathbf{r}_2)\varphi_k(\mathbf{r}_3)$, the bias field b can then be approximated as

$$b(\mathbf{r})=\sum_{i=0}^{K}\sum_{j=0}^{K}\sum_{k=0}^{K}c_{i,j,k}\Phi_{i,j,k}(\mathbf{r})$$

or, more concisely, as $b(\mathbf{r})=\Phi(\mathbf{r})c$. Consequently, the problem of estimation of the bias field b can be reduced to the equivalent problem of estimation of its polynomial coefficients $c\in\mathbb{R}^{(K+1)^3}$. In this case, the optimization problem (5) becomes

$$\min_{\xi,\mu_d,\mu_f,c}\Bigg\{\lambda_d\sum_{\mathbf{r}\in\Omega}\xi(\mathbf{r})|g(\mathbf{r})-\mu_d-\Phi(\mathbf{r})c|^2+\lambda_f\sum_{\mathbf{r}\in\Omega}(1-\xi(\mathbf{r}))|g(\mathbf{r})-\mu_f-\Phi(\mathbf{r})c|^2+ \\ +\ \|\xi\|_{\mathrm{TV}}+I_{[0,1]}(\xi)\Bigg\}. \tag{6}$$

In this work, to define $\Phi(\mathbf{r})$, Bernstein polynomials have been used [19]. This choice is by no means exclusive, and alternative definitions of polynomial bases could have been used instead.

2.3 Numerical Solution

While much more tractable compared with its original version, the optimization problem (6) can still benefit further simplifications. To this end, one can first split the (optimization) variables to yield an equivalent problem of the form

$$\min_{\xi,\mu_d,\mu_f,c}\Bigg\{\lambda_d\sum_{\mathbf{r}\in\Omega}\xi(\mathbf{r})|g(\mathbf{r})-\mu_d-\Phi(\mathbf{r})c|^2+\lambda_f\sum_{\mathbf{r}\in\Omega}(1-\xi(\mathbf{r}))|g(\mathbf{r})-\mu_f-\Phi(\mathbf{r})c|^2+ \\ +\ \|\eta\|_{\mathrm{TV}}+I_{[0,1]}(\xi)\Bigg\},\quad \text{s.t. } \xi=\eta. \tag{7}$$

In this case, the augmented Lagrangian of the new problem can be defined as

$$\begin{aligned}\mathcal{L}(\xi,\eta,\mu_d,\mu_f,c,y) &= \\ = \lambda_d \sum_{\mathbf{r}\in\Omega} \xi(\mathbf{r})|g(\mathbf{r}) - \mu_d - \Phi(\mathbf{r})c|^2 + \lambda_f \sum_{\mathbf{r}\in\Omega} (1-\xi(\mathbf{r}))|g(\mathbf{r}) - \mu_f - \Phi(\mathbf{r})c|^2 + \\ + \|\eta\|_{\mathrm{TV}} + I_{[0,1]}(\xi) + \frac{\delta}{2}\sum_{\mathbf{r}\in\Omega} |\xi(\mathbf{r}) - \eta(\mathbf{r}) + y(\mathbf{r})|^2, \qquad (8)\end{aligned}$$

where y denotes a scaled version of the vector of Lagrange multipliers and $\delta > 0$ is a smoothing parameter (e.g., $\delta = 0.5$).

At this point, one can use the Alternating Directions Method of Multipliers (ADMM) [16] to minimize $\mathcal{L}(\xi,\eta,\mu_d,\mu_f,c,y)$ with respect to the primal variables (i.e., w.r.t. ξ, η, μ_d, μ_f, and c) *iteratively* using the following steps.

- Step 1: $\xi^{t+1} = \arg\min_{\xi} \mathcal{L}(\xi, \eta^t, \mu_d^t, \mu_f^t, c^t, y^t)$
- Step 2: $\eta^{t+1} = \arg\min_{\eta} \mathcal{L}(\xi^{t+1}, \eta, \mu_d^t, \mu_f^t, c^t, y^t)$
- Step 3: $(\mu_d^{t+1}, \mu_f^{t+1}, c^{t+1}) = \arg\min_{\mu_d,\mu_f,c} \mathcal{L}(\xi^{t+1}, \eta^{t+1}, \mu_d, \mu_f, c, y^t)$

Once the primary variables have been updated, the dual variable y is updated according to

$$y^{t+1}(\mathbf{r}) = y^t(\mathbf{r}) + \xi^{t+1}(\mathbf{r}) - \eta^{t+1}(\mathbf{r}), \quad \forall \mathbf{r} \in \Omega.$$

Although the number of update steps above could look prohibitively large at the first glance, they all admit either closed-form or efficiently solutions, which considerably reduces the cost of each ADMM iteration. Specifically, the updates can be performed as follows.

Solution to Step 1. The update in ξ requires solving a simple quadratic minimization problem, followed by orthogonally projecting its solution onto the interval $[0,1]$. Moreover, the update can be performed separately at each $\mathbf{r}$ according to

$$\xi(\mathbf{r})^{t+1} = \Pi_{[0,1]}\left\{\eta^t(\mathbf{r}) - y^t(\mathbf{r}) + \frac{\lambda_f - \lambda_d}{\delta}\Big(g(\mathbf{r}) - (\mu_f^t - \mu_d^t) - \Phi(\mathbf{r})c^t\Big)\right\},$$

where $\Pi_{[0,1]}(z) = \max\{\min\{z,1\},0\}$ denotes the operator of orthogonal projection onto $[0,1]$.

Solution to Step 2. The update in η requires solving a norm minimization problem of the form

$$\eta^{t+1} = \arg\min_{\eta}\left\{\frac{1}{2}\sum_{\mathbf{r}\in\Omega} |\eta(\mathbf{r}) - (\xi^{t+1}(\mathbf{r}) + y^t(\mathbf{r}))|^2 + \frac{1}{\delta}\|\eta\|_{\mathrm{TV}}\right\}.$$

This problem has the format of well-known *TV de-noising* [20], which can be efficiently solved by a number of numerical methods. In this work, to solve this problem, the fixed-point algorithm of [21] has been used.

Solution to Steps 3. To derive an equation for the update of μ_d, μ_f and c, it is convenient to think of $\Phi(\mathbf{r})$ as an $N \times M$ matrix, with N equal to the number of voxels in Ω and $M = (K+1)^3$ being the total number of polynomial coefficients used for representation of b. In an analogous manner, both g and ξ^{t+1} can be also thought of as column vectors of length N, with a similar interpretation of c as a length M (column) vector.

Using the notational simplifications above, let $\theta \in \mathbb{R}^{M+2}$ be a new vector obtained via concatenation of μ_d, μ_f and c, namely $\theta = [\mu_d, \mu_f, c^T]^T$. Also, let A_d and A_f be two $N \times (M+2)$ matrices obtained by augmenting Φ with a zero $\mathbf{0}$ and a unit $\mathbf{1}$ column as $A_d = [\mathbf{1}\,\mathbf{0}\,\Phi]$ and $A_f = [\mathbf{0}\,\mathbf{1}\,\Phi]$, respectively. Finally, let W_d and W_f be two diagonal matrices defined by vectors $\lambda_d\,\xi^{t+1}$ and $\lambda_d\,(1-\xi^{t+1})$, correspondingly, as well. Then, with

$$B = A_d^T W_d A_d + A_f^T W_f A_f \quad \text{and} \quad \beta = (A_d^T W_d + A_f^T W_f) g,$$

the optimal value of θ can be shown to be a solution to the linearly constrained quadratic program given by

$$\arg\min_{\theta}\ \theta^T B \theta - 2\beta^T \theta, \quad \text{s.t. } e^T \theta = 0, \tag{9}$$

with $e \in \mathbb{R}^{M+2}$ of the form $e = [1, 1, 0, 0, \ldots, 0]^T$. Note that the constraint $\nu^T \theta = 0$ is added to guarantee the attainment of a solution with $\mu_d \neq \mu_f$, thus enforcing the photometric discrepancy between the dense and fat tissues.

When applied to the constrained problem in (9), the Karush-Kuhn-Tucker optimality conditions result in a system of linear equations in the primal optimal θ^* and the dual optimal ν^* variables that is given by [22]

$$\begin{bmatrix} B & e \\ e^T & 0 \end{bmatrix} \begin{bmatrix} \theta^* \\ \nu^* \end{bmatrix} = \begin{bmatrix} \beta \\ 0 \end{bmatrix}. \tag{10}$$

The above system of equation is straightforward to solve to find θ^*, from which the values of μ_d^{t+1}, μ_f^{t+1}, and c^{t+1} can be extracted.

2.4 Algorithm Convergence

In a series of both computer simulations and experiments with real-life breast MRI data, the proposed algorithm has demonstrated stable and consistent convergence in less than 20 iterations, using $\lambda_d = \lambda_f = 0.1$ and $\delta = 0.5$. Once the optimal ξ^* was computed, its corresponding domain partition/segmentation was defined as

$$\Omega_d = \{\mathbf{r} \in \Omega \mid \xi^*(\mathbf{r}) \geq 0.5\} \quad \text{and} \quad \Omega_f = \{\mathbf{r} \in \Omega \mid \xi^*(\mathbf{r}) < 0.5\}.$$

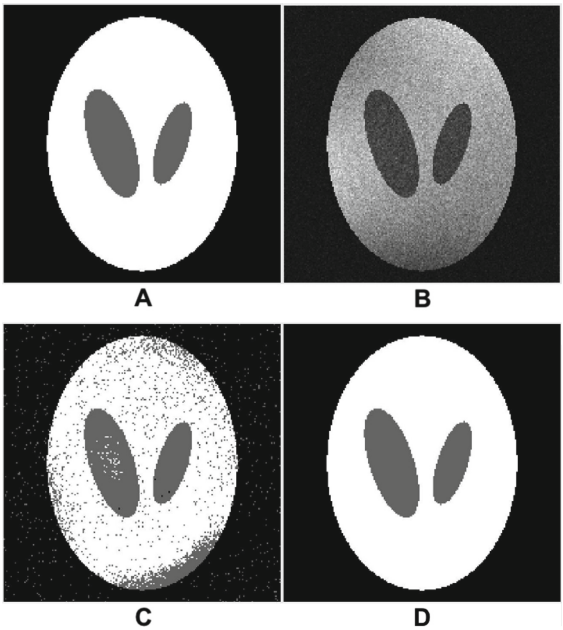

Fig. 2. (Subplot A) Cross-sectional slice of a 3-D phantom; (Subplot B) Same slice contaminated by a bias field and Rician noise; (Subplot C) Segmentation obtained using the GMM-based method of [18]; (Subplot D) Segmentation obtained using the proposed method.

3 Experimental Results

The performance of the proposed method for segmentation of breast MRI scans has been tested using both phantom and real-life data. In the former case, a 3-D version of the Shepp-Logan phantom has been used as a model of the breast, while in the latter case we used the breast MRI scans acquired with a 3T Signa^{TM} Premier MRI scanner (GE Healthcare, Inc.) at the Princess Margaret Cancer Center (Toronto, Canada). As a reference method, the GMM-based algorithm of [18] has been used.

Some representative results produced by the reference and proposed methods are shown in Figs. 2 and 3 corresponding to the case of *in silico* and *in vivo* experiments, respectively. One can see that the Gaussian model is incapable of adequately capturing the nature of Rician noise, resulting in erroneous segmentation. The proposed method, on the other hand, has been able to produce valuable results at low SNR and in the presence of sizable bias.

Moreover, using the phantom data allowed us to compare the performance of the reference and proposed methods in a quantitative way. As a figure of merit,

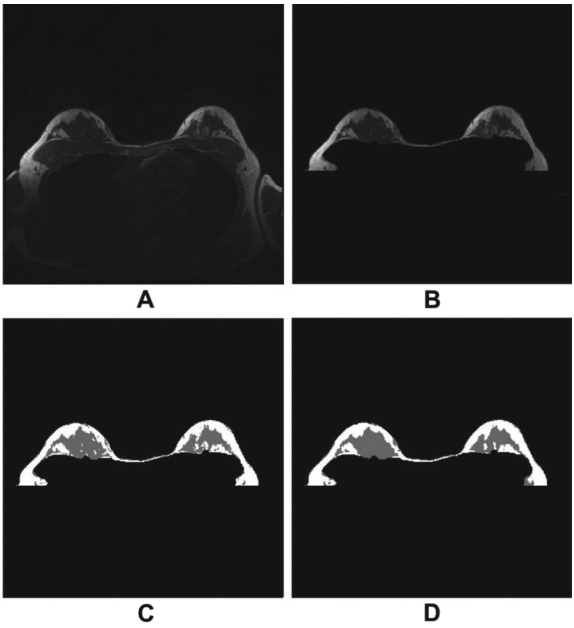

Fig. 3. (Subplot A) Axial slice of a 3-D breast MRI volume; (Subplot B) Same slice contaminated by a bias field and Rician noise; (Subplot C) Segmentation obtained using the GMM-based method of [18]; (Subplot D) Segmentation obtained using the proposed method.

we used the Dice Similarity Coefficient (DCS) which is defined as

$$\mathrm{DSC} = \frac{2|X \cap Y|}{|X| + |Y|},$$

where X and Y denote two non-empty sets of size $|X|$ and $|Y|$, respectively. Note that, with X being the true Ω_d (or, alternatively, Ω_f) and Y being its estimate, the values of DCS are distributed between 0 and 1, with the latter corresponding to the case of perfect segmentation.

Table 1. Quantitative comparison of the reference and proposed methods.

SNR(in dB)	DSC (reference method)	DSC (proposed method)
6.6	0.86	0.97
7.0	0.65	0.94
7.4	0.65	0.91
7.8	0.69	0.95
12.0	0.86	0.97
12.3	0.79	0.97

The quantitative comparisons have been performed at different levels of SNR and bias field contamination. Table 1 demonstrates the obtained results for a representative set of SNR values. One can see that, in all these cases, the proposed method outperforms the reference segmentation by a substantial margin.

4 Conclusion

In this work, a new method of segmentation of breast MRI scans has been described. A principle attribute of the method is its formulation in the logarithmic domain in conjunctions with proper "gaussianization". It has been shown that such preprocessing allows on to substantially simplify the problem of image segmentation, leading to a computationally efficient numerical solution that remains accurate and stable for a wide range of values of SNR as well as in the presence of sizable bias fields.

References

1. Monticciolo, D.L., Newell, M.S., Moy, L., Niell, B., Monsees, B., Sickles, E.A.: Breast cancer screening in women at higher than average risk: recommendations from the ACR. J. Am. Coll. Radiol. **15**(3), 408–414 (2018)
2. Plana, M.N., et al.: Magnetic resonance imaging in the preoperative assessment of patients with primary breast cancer: systematic review of diagnostic accuracy and meta-analysis. Eur. Radiol. **22**(1), 26–38 (2012)
3. Song, H., Cui, X., Sun, F.: Tissue 3D segmentation and visualization on MRI. Int. J. Biomed. Imaging (2013). Article ID 859746
4. Fooladivanda, A., Shokouhi, S.B., Mosavi, M.R., Ahmadinejad, N.: Atlas-based automatic breast MRI segmentation using pectoral muscle and chest region model. In: ICBME (2014)
5. Raba, D., Oliver, A., Martí, J., Peracaula, M., Espunya, J.: Breast segmentation with pectoral muscle suppression on digital mammograms. In: Marques, J.S., Pérez de la Blanca, N., Pina, P. (eds.) IbPRIA 2005. LNCS, vol. 3523, pp. 471–478. Springer, Heidelberg (2005). https://doi.org/10.1007/11492542_58
6. Kannan, S.R., Ramathilagam, S., Sathya, A.: Robust fuzzy C-means in classifying breast tissue regions. In: ARTCom 2009, pp. 543–545 (2009)
7. Niukkanen, A., et al.: Quantitative volumetric K-means cluster segmentation of fibroglandular tissue and skin in breast MRI. J. Digit. Imaging **31**(4), 425–434 (2018)
8. Pathmanathan, P.: Predicting tumour location by simulating the deformation of the breast using nonlinear elasticity and the finite element method. Doctoral dissertation, Wolfson College University of Oxford (2006)
9. Nie, K., et al.: Development of a quantitative method for analysis of breast density based on three dimensional breast MRI. Med. Phys. **35**(12), 5253–5262 (2008)
10. Dalmış, M.U., et al.: Using deep learning to segment breast and fibroglandular tissue in MRI volumes. Med. Phys. **44**(2), 533–546 (2017)
11. Han, L., et al.: A nonlinear biomechanical model based registration method for aligning prone and supine MRI breast images. IEEE Trans. Med. Imaging **33**(3), 682–694 (2014)

12. Gubern-Merida, A., Kallenberg, M., Mann, R.M., Marti, R., Karssemeijer, N.: Breast segmentation and density estimation in breast MRI: a fully automatic framework. IEEE J. Biomed. Health Inform. **19**(1), 349–357 (2015)
13. Dempster, A.P., Laird, N.M., Rubin, D.B.: Maximum likelihood from incomplete data via the EM algorithm. J. Roy. Stat. Soc. B (Methodol.) **39**(1), 1–38 (1977)
14. Gudbjartsson, H., Patz, S.: Rician distribution of noisy MRI data. Magn. Reson. Med. **34**(6), 910–914 (1995)
15. Leys, C., Ley, C., Klein, O., Bernard, P., Licata, L.: Detecting outliers: do not use standard deviation around the mean, use absolute deviation around the median. J. Exp. Soc. Psychol. **49**(4), 764–766 (2013)
16. Boyd, S., Parikh, N., Chu, E., Peleato, B., Eckstein, J.: Distributed optimization and statistical learning via the alternating direction method of multipliers. Found. Trends Mach. Learn. **3**(1), 1–122 (2011)
17. Juntu, J., Sijbers, J., Van Dyck, D., Gielen, J.: Bias field correction for MRI images. In: Kurzyński, M., Puchała, E., Woźniak, M., Żołnierek, A. (eds.) Computer Recognition Systems. AINSC, vol. 30, pp. 543–551. Springer, Heidelberg (2005). https://doi.org/10.1007/3-540-32390-2_64
18. Mory, B., Ardon, R., Thiran, J.P.: Variational segmentation using fuzzy region competition and local non-parametric probability density functions. In: ICCV, pp. 1–8 (2007)
19. Lorentz, G.G.: Bernstein Polynomials. American Mathematical Society, Providence (2013)
20. Rudin, L.I., Osher, S., Fatemi, E.: Nonlinear total variation based noise removal algorithms. Physica D **60**(1–4), 259–268 (1992)
21. Chen, D.Q., Zhang, H., Cheng, L.Z.: A fast fixed point algorithm for total variation deblurring and segmentation. J. Math. Imaging Vis. **43**(3), 167–179 (2012)
22. Boyd, S., Vandenberghe, L.: Convex Optimization. Cambridge University Press, Cambridge (2004)